RSC Advances

ROYAL SOCIETY OF CHEMISTRY

www.rsc.org/advances

Journal Name

RSCPublishing

COMMUNICATION

Polybenzoxazine Aerogels with Controllable Pore Structures

Cite this: DOI: 10.1039/xoxxoooooox

Senlong Gu,[a] Zhen Li,[b] Toshikazu Miyoshi [b] and Sadhan C. Jana[*a]

Received ooth January 2012,
Accepted ooth January 2012

DOI: 10.1039/xoxxoooooox

www.rsc.org/

Abstract: Time-efficient gelation of benzoxazine using p-toluenesulfonic acid (TSA) as the catalyst in several solvents and controllable pore structure formation in resultant polybenzoxazine (PBZ) aerogels are reported. The aerogel building blocks (spheres vs. strands) and the pore surface area show strong dependence on the solvent and the gelation temperature.

Aerogels are three-dimensional highly porous networks of solids with the pores filled with air. They are obtained from the corresponding precursor gels by replacing the liquid with air.[1-6] The precursor gels are synthesized via thermo-reversible gelation process[4-6] or by sol-gel chemistry.[1-3] It is interesting to note that aerogels are open-celled materials with micro-, meso-, or macropores with pore sizes respectively less than 2 nm, 2-50 nm, and greater than 50 nm and offer extremely high specific surface area.[3]

In last two decades, carbon aerogels received considerable attention triggered by its micro- and meso-porous carbon network structures, excellent electrical conductivity, and widespread application potential in sorption, catalysis, acoustic/thermal insulators, and electrode materials. In 1989, first carbon aerogel was prepared via pyrolysis of organic aerogel synthesized from condensation of resorcinol-formaldehyde (RF).[7, 8] Recently, researchers reported nitrogen-doped (N-doped) carbon aerogels with superior performance as CO_2 absorbent[9] and as electro-catalyst for oxygen reduction reactions.[10, 11] A suitable way to produce N-doped carbon aerogel is to add nitrogen containing molecules into RF condensation process.[12, 13] Meanwhile, the N-containing structure of benzoxazine (BZ) was exploited by many researchers in synthesis of N-doped carbon materials using polybenzoxazine (PBZ) as the precursor.[14-17]

Polybenzoxazines represent a class of phenolic resins with a number of unique characteristics, such as high mechanical strength, near-zero shrinkage upon polymerization of its monomer, and high char yield.[18] Interestingly, ring-opening polymerization of BZ in solvents leads to gelation and formation of three-dimensional polymer networks. Lorjai et al. first reported the synthesis of PBZ gels by thermally-induced ring opening polymerization of BZ in xylene at 130 ºC.[14] Recently, Mahadik-Khanolkar et al.[16] published a new method for preparation of PBZ gels at room temperature by using hydrochloric acid as the catalyst of cationic ring opening polymerization. The scanning electron microscopy images revealed that the corresponding aerogels consisted of spherical polymer particles as the building block and that the diameter of spherical particles reduced with an increase in the concentration of BZ in solution.

In this letter, we present an alternative method of preparation of PBZ gels in various solvents using p-toluenesulfonic acid (TSA) as the catalyst and study the effects of polymerization temperature and the

type of solvent on pore structure, porosity, and surface area of PBZ aerogels. Benzoxazine monomer used in this work was synthesized from bisphenol A, aniline, and paraformaldehyde.[19] The mechanism of ring-opening polymerization of BZ into PBZ in the presence of TSA was proposed by Chutayothin and Ishida[20] as shown in Scheme S1. The addition of TSA (2% w/w of BZ) to a solution of BZ in DMSO (0.275 g/mL BZ) reduced the time of gelation to approximately 10 min at 130 ºC. In comparison, the time of gelation was 12 h at 130 ºC without any catalyst.[14, 16] It is noted that the gel time is a function of specimen size and is dependent on the speed of heat transfer from the heating medium. In this work, the gel time is reported for a solution of 10 g at a fixed concentration of 0.275 g/mL of BZ. Details of sample preparation method are provided in the supporting information.

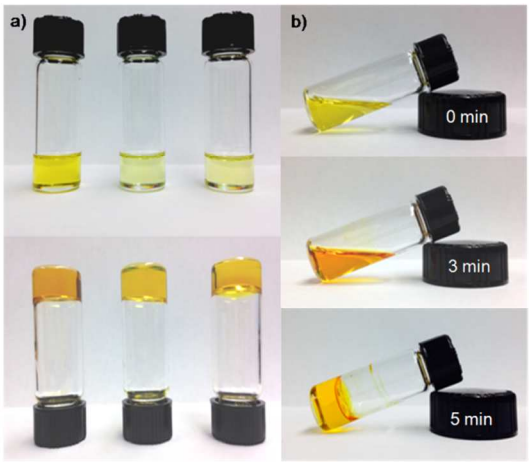

Figure 1. Column (a): PBZ gels formed in different solvents by heating at 130 ºC in solvents (left to right) DMSO, DMA, and NMP. Column (b): State of the liquid by heating BZ/DMSO solution at 130 ºC for 0 min, 3 min, and 5 min.

Figure 1 presents the states of BZ solutions before and after heating at 130 °C. In Figure 1(a), the top row presents the images of the solutions and the bottom row shows that the materials turned into gels. In Figure 1(b), the states of the solution at three different times are shown. It is noted that the colour of the materials became much darker once the gels were formed.

Figure S1 shows the viscosity vs. time plots of BZ sols allowed to gel at 90 °C and 130 °C. The gel time was recorded as the time when the viscosity diverged. The gel times were found approximately 580 s for material BZ/DMSO solution heated at 130 °C, 59 min for BZ/DMSO solution heated at 90 °C, 63 min for BZ/NMP solution heated at 130 °C, and 218 min for BZ/NMP solution heated at 90 °C. The results imply that BZ formed gels the quickest in DMSO, e.g., in approximately 10 min compared to 63 min in NMP at 130 ºC. Intuitively, the gel time shortened at higher temperature, e.g., gels were formed in 59 min at 90 °C and in 10 min at 130 °C in DMSO. The gels were solvent exchanged with liquid carbon dioxide and dried under supercritical condition of carbon dioxide to obtain the aerogels. The specimens are designated as "PBZ-s-T", where "s" represents the solvent used and "T" represents the gelation temperature. For example, the specimen PBZ-DMSO-130 refers to PBZ aerogel synthesized in DMSO solvent at 130 °C. The aerogels were not subjected to further curing.

The aerogels reported in literature to date can be classified into three skeletal frameworks – (1) aggregates of spheres, e.g., those found in silica aerogels[21, 22] and some polymeric aerogels, (2) fibrillar networks, e.g., the crystalline strands found in syndiotactic polystyrene aerogel[5, 23] or the phase separated amorphous polymer strands in polyimides, polyurea and polydicyclopentadiene,[24-28] or (3) aggregates of layered structures, e.g., the ones found in clay aerogels.[29] Intuitively, these frameworks offer differences in specific surface area, pore size, and mechanical strength.[23, 26, 30] In this study, the skeletal framework of PBZ aerogels was revealed using scanning electron microscope (SEM) images. As highlighted in Figure 2, PBZ-DMSO-130 and PBZ-DMA-130 aerogels are composed of aggregates of spheres of diameters 43.5± 3.0 nm and 49.2 ± 6.9 nm, respectively. However, the primary frameworks of PBZ-NMP-130 aerogel are polymer strands of diameter of 32.1± 3.3 nm, shown in Figure 2(c). The diameter values quoted above represent the averages of 10 individual measurements taken at random locations of the corresponding SEM images. Recall that these frameworks originated during gelation via polymerization-induced phase separation of the polymer. We now present a plausible argument to explain the formation of different building blocks identified in Figure 2 by making two general statements. First, a strand-like morphology as in Figure 2c can result only if phase separation occurred via spinodal decomposition. Second, the morphology with spherically connected domains, as in Figure 2a and Figure 2b, can result from nucleation and growth, spinodal decomposition, or a combination of spinodal decomposition followed by nucleation and growth. Yamanaka and Inoue[31] studied reaction-induced phase separation of crosslinked epoxy domains in poly(ether sulfone) and identified that interconnected globular domains of epoxy resulted from spinodal decomposition. In light of rapid gelation observed in

our experimental system, as reflected from the large values of slope of viscosity vs. time plots in Figure S1, we believe that phase separation proceeded via spinodal decomposition and yielded co-continuous solid network structures. The viscosity vs. time slopes around gel time varied from 5-400 cP/s in our system. The just phase-separated domains quite possibly continued to evolve with time, e.g., via phase coarsening or shape relaxation into spherical globules. A thorough investigation is needed to determine the set of factors that govern the morphological differences seen in Figure 2. This, however, is beyond the scope of this letter.

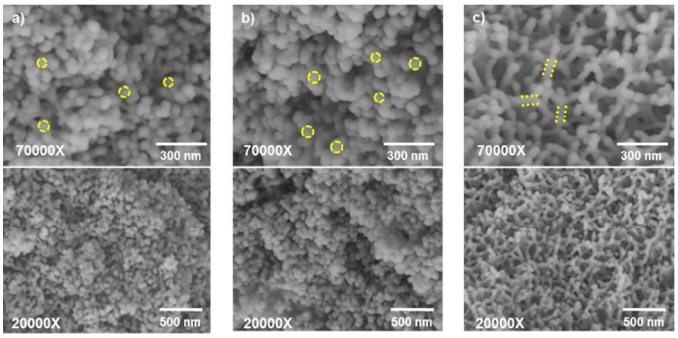

Figure 2. SEM images at 20,000× and 70,000× magnification of aerogel specimens (a) PBZ-DMSO-130, (b) PBZ-DMA-130, (c) PBZ-NMP-130.

The data from infrared (IR) and nuclear magnetic resonance (NMR) spectroscopy are now analysed. The objective is to evaluate if the nature of polymer chains differed significantly from what is published literature or significant chain fusion occurred at higher reaction temperature. These are important considering that TSA was used as the catalyst and that polymerization was carried out 90 °C and 130 °C in different solvents. The curves in Figure 3 present the IR spectra of BZ and PBZ, which were analysed in reference to the existing IR data on ring-opening polymerization of BZ.[16, 32, 33] All specimens show broad absorbance in the range 3090 cm^{-1}-3465 cm^{-1} which are attributed to stretching of the phenolic O-H groups. In addition, the peak at 940 cm^{-1} associated with the oxazine ring of BZ monomer is weak in all PBZ specimens. The peaks at 1230 cm^{-1} and 1029 cm^{-1} due to asymmetric stretching of Ph-O-C groups are absent and the peak due to phenolic Ph-O group at 1248 cm^{-1} [33] is visible. Thus, the polymer chains obtained at different temperatures and using different solvents do not show distinctive features. However, the spectra in Figure 3 indicate that the gelation temperature had some influence on incorporation of the aniline moieties present in BZ monomer. In this context, the absorbance peaks at 693 cm^{-1} and 750 cm^{-1} in the spectra of BZ monomer are attributed to out-of-plane (OOP) C-H bending vibrations from dangling aniline.[34] It is seen that the peak at 693 cm^{-1} became much weaker for PBZ-DMSO-90 and PBZ-NMP-90 aerogel specimens and nearly disappeared in aerogel specimens PBZ-DMSO-130 and PBZ-NMP-130. Thus, we infer that the aniline moiety participated in the gelation process of BZ at both 90 °C and 130 °C and that its incorporation into gel structure was complete at 130 °C.

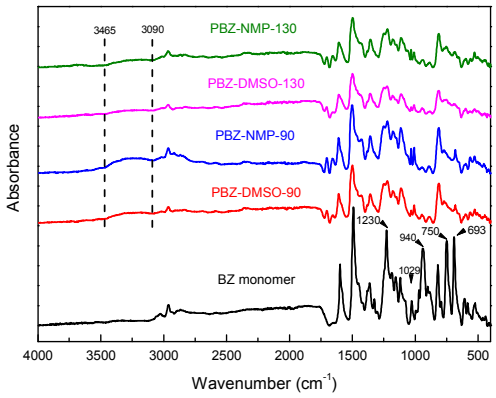

Figure 3. Infrared (IR) spectra of BZ monomer and PBZ aerogels.

Solid-State NMR (SS-NMR) is a useful tool to reveal the molecular structures and the dynamics in polymer and supra-molecular systems.[35-39] High resolution SS-NMR spectrum for BZ monomer is shown by the bottom black curve in Figure 4. The high resolution SS-NMR spectra show well separated chemical groups except in the benzene ring region. These chemical shifts correlate well with the solution NMR spectrum.[16] With the use of high magic angle spinning (MAS) rate of 12000 Hz, the spinning sidebands were suppressed and out of the spectrum range. The peaks from benzene rings appear at 100 to 160 ppm, which can further be divided into two parts. The benzene ring directly connected to O, N and -$C(CH_3)_2$ is shown above 137 ppm and can be well separated as in Figure 4. The peaks and the corresponding chemical structures are labelled in the structure of BZ presented in scheme S2. The rest of the carbons on the benzene rings appear below 137 ppm and the signals show much overlap. The peak at 80 ppm is well isolated and assigned to the carbon labelled ***d*** in scheme S2. The three peaks in between 20-40 ppm can be assigned to the ***a*** to ***c*** aliphatic carbons. Although the peak intensity of each peak relies on cross polarization (CP) efficiency, the peak intensity correlates well with the chemical groups and the number of carbon atoms in BZ monomer.

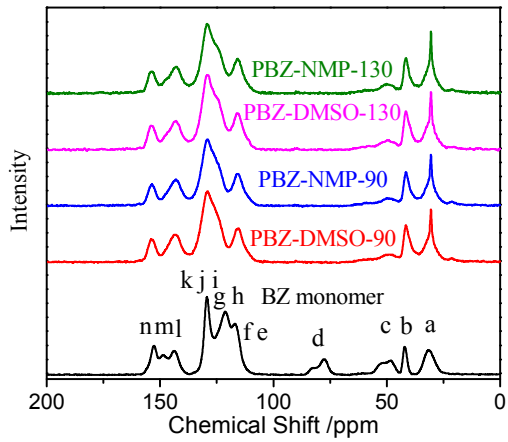

Figure 4. ^{13}C-NMR spectra of samples for BZ monomer and the polymers at different conditions.

The spectra for aerogel specimens are also shown in Figure 4. All the spectra of PBZ show the absence of resonance at 80 ppm (carbon ***d***) indicating the breakup of C-O bonds of oxazine rings during polymerization. The spectra for PBZ-DMSO-90 and PBZ-NMP-90 are identical which means that the same chemical structures were obtained in different solvents. The PBZ-DMSO-130 and PBZ-NMP-130 also show identical line shapes but slight differences are evident at 125 ppm. The shoulder peaks from PBZ-DMSO-130 and PBZ-NMP-130 are more apparent than those of PBZ-DMSO-90 and PBZ-NMP-90. Another important resonance to note is the peak at 50 ppm. After polymerization, the reacted carbon ***d*** is supposed to move to 50 ppm (carbon ***p*** in Scheme S2). The intensity of this peak of PBZ aerogel synthesized at 130 °C is higher than that synthesized at 90 °C. It means higher conversion of BZ into PBZ in aerogel specimens PBZ-DMSO-130 and PBZ-NMP-130. In view of the IR data and NMR data we infer that the PBZ molecules obtained with TSA as the catalyst resemble the structure reported in Scheme S2.

We now examine if the small differences in characteristic dimension of the polymer frameworks (sphere and strands) seen in Figure 2 lead to any differences in surface area. The surface area and pore size distribution of the aerogel specimens were determined from nitrogen sorption porosimetry using Micromeritics Tristar II 3020 Analyzer. The nitrogen adsorption-desorption isotherms show hysteresis loops in Figure 5a, signifying the presence of mesopores. Specifically, the hysteresis loops of the isotherms of aerogel specimens PBZ-DMSO-130 and PBZ-DMA-130 can be categorized under IUPAC classification Type H2 signifying that the mesopores in these specimens were created by the aggregation of spheres.[40] In contrast, the desorption curve of PBZ-NMP-130 aerogel does not show a plateau at high value of P/P_0 (see inset of Figure 5a). In this case, the hysteresis loop is closer to Type H3. This observation corroborates the visual evidence of SEM image in Figure 2c that the pores created in this aerogel are due to fibrillar polymer frameworks.

The much wider hysteresis loop of PBZ-DMSO-130 aerogel in Figure 5a indicates that the pores in this aerogel specimen should be predominantly mesopores. This is supported by the data on pore size distribution in Figure 5b obtained using Barrett-Joyner-Halenda (BJH) method. The red and blue curves in Figure 5b confirm the existence of bimodal mesopores in PBZ-DMA-130 and PBZ-NMP-130 aerogels.

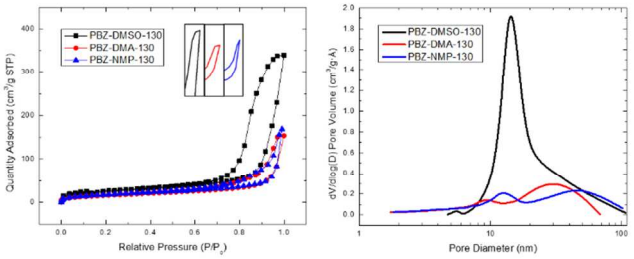

Figure 5. (a) Nitrogen adsorption-desorption isotherms and (b) pore size distribution of PBZ aerogels. The inset in (a) shows the hysteresis loops of three isotherms at high P/P_0.

Another factor studied is the influence of gelation temperature on the pore structures of PBZ aerogels. For this purpose, the gels synthesized in DMSO as well as NMP at 90 ºC and 130 ºC were considered. It is apparent from SEM images presented in Figure 6a and 6b that both PBZ-DMSO-130 and PBZ-DMSO-90 aerogel specimens are constituted of similar size aggregates of polymer spheres. In contrast, PBZ-NMP-90 and PBZ-NMP-130 show the fibrillar networks. The SEM images demonstrate that the skeletal network of PBZ aerogel is dependent on the solvent instead of the gelation temperature. Further evidence could be derived from the nitrogen adsorption-desorption isotherms in Figure 7. Figure 7a clearly shows two Type IV isotherms. PBZ-DMSO-90 has a perfect Type H1 hysteresis loop indicating that the network is composed of approximately uniform spheres in fairly regular array. However, the hysteresis loop of PBZ-DMSO-130 is closer to Type H2 as discussed in the previous section. As a result, the pore size

distribution for PBZ-DMSO-90 aerogel specimen exhibits narrower peak and a significant fraction of smaller mesopores (mean diameter ~10.2 nm, Table 1) than PBZ-DMSO-130 aerogel specimen (mean diameter ~19.1 nm, Table 1). The nitrogen adsorption-desorption isotherms of PBZ-NMP-90 and PBZ-NMP-130 are both Type IV isotherms with Type H3 hysteresis loops. Similarly, PBZ-NMP-90 possesses higher surface area and smaller mean pore diameter than PBZ-NMP-130 (Table S1). PBZ aerogels prepared at 130 °C show lower BET surface area than the ones prepared at 90 °C independent of the solvents used.

Table 1.Properties of PBZ-DMSO-130 and PBZ-DMSO-90 aerogel specimens.

Specimen	BET surface area (m^2/g)	Pore volume $V_{1.7\text{-}300\ nm}$ (cm^3/g)	Predominant pore diameter (nm)	Calculated specific surface area (A_{est}) (m^2/g)
PBZ-DMSO-130	99.5	0.63	19.1	99.0
PBZ-DMSO-90	129.6	0.54	10.2	158.8

In view of the data presented in Table 1 and Table S1, the higher BET surface area of PBZ-DMSO-130 and PBZ-DMSO-90 specimens can be attributed to relatively higher pore volume $V_{1.7\text{-}300\ nm}$. The pore volume $V_{1.7\text{-}300\ nm}$ in Table 1 refers to the cumulative volume of pores of diameter between 1.7 and 300 nm. It is however, intriguing to find that PBZ-DMSO-130 aerogel specimen with higher value of $V_{1.7\text{-}300\ nm}$ (0.63 cm^3/g) has lower surface area (99.5 m^2/g) than PBZ-DMSO-90 aerogel specimen with smaller pore volume (0.54 cm^3/g) but higher BET surface area (129.6 m^2/g). As discussed earlier, aerogel specimens PBZ-DMSO-130 and PBZ-DMSO-90 contained predominant mesopores with diameter in the range 2-50 nm, with the peak values of 19.1 nm for PBZ-DMSO-130 and 10.2 nm for PBZ-DMSO-90. If one assumes that all pores have diameter the same as the peak diameter, the specific surface area (A_{est}) can be estimated using equation 1:

$$A_{est} = \frac{3V_{1.7-300nm}}{R_p} \qquad (1)$$

In equation 1, $V_{1.7\text{-}300\ nm}$ is the pore volume and R_p is the peak pore radius. It is evident from Table 1, the estimated area of PBZ-DMSO-90 is almost 160% as much as the value for PBZ-DMSO-130 aerogel. This calculation supports that the much smaller pore diameter of PBZ-DMSO-90 aerogel specimen more than compensates for the lower pore volume in producing higher BET surface area.

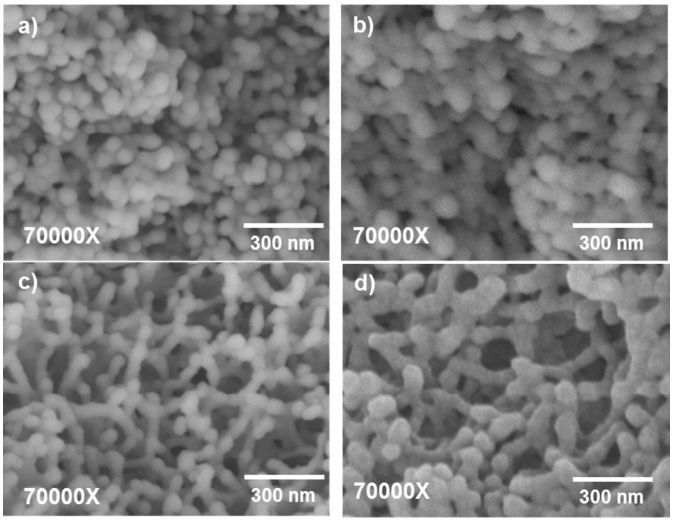

Figure 6. SEM images of (a) PBZ-DMSO-130, (b) PBZ-DMSO-90, (c) PBZ-NMP-130, (d) PBZ-NMP-90.

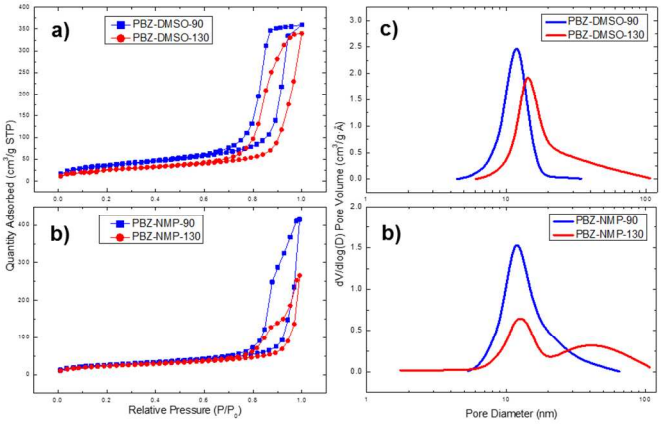

Figure 7. Nitrogen adsorption-desorption isotherms of (a) PBZ-DMSO-90/130, (b) PBZ-NMP-90/130 and pore size distribution of (c) PBZ-DMSO-90/130, (d) PBZ-NMP-90/130.

Conclusions

In summary, we demonstrated a time efficient preparation of PBZ aerogel using TSA as the catalyst. All of the aerogels synthesized in

DMSO, DMA, and NMP were found to be mesoporous materials. Interestingly, the study revealed that the skeletal frameworks of PBZ aerogels can be tuned using appropriate solvents and suitable polymerization temperature. The use of DMSO and DMA as the solvents led to spherical particle networks while fibrillar networks were obtained using NMP. The temperature of polymerization played critical role in controlling the pore structures of PBZ aerogels. Of the aerogels studied, PBZ-DMSO-90 specimens exhibited the largest BET surface area owing to predominantly mesopores with peak diameter of ~10 nm. It is anticipated that such vast changes in pore structures and pore surface area due to use of different solvents and polymerization temperature can be efficiently captured in the design of other polymeric aerogels.

Notes and references

[a] *Department of Polymer Engineering, University of Akron, 250 S Forge St, Akron, OH 44325-0301, USA. E-mail: janas@uakron.edu; Fax: +3309723406; Tel: +3309728293*

[b] *Department of Polymer Science, The University of Akron, Akron, Ohio 44325-3909, United States*

1 S. S. Kistler, *Nature*, 1931, **127**, 741-741.
2 C. J. Brinker and G. W. Scherer, *J. Non-Cryst. Solids*, 1985, **70**, 301-322.
3 J. Fricke, *J. Non-Cryst. Solids*, 1988, **100**, 169-173.
4 Y. Chatani, Y. Shimane, T. Inagaki, T. Ijitsu, T. Yukinari and H. Shikuma, *Polymer*, 1993, **34**, 1620-1624.
5 C. Daniel, D. Alfano, V. Venditto, S. Cardea, E. Reverchon, D. Larobina, G. Mensitieri and G. Guerra, *Adv. Mater.*, 2005, **17**, 1515-1518.
6 C. Daniel, C. Dammer and J.-M. Guenet, *Polymer*, 1994, **35**, 4243-4246.
7 R. W. Pekala, J. Mater. Sci., 1989, **24**, 3221-3227.
8 N. P. Wickramaratne, J. Xu, M. Wang, L. Zhu, L. Dai and M. Jaroniec, *Chem. Mater.*, 2014, **26**, 2820-2828.
9 G. P. Hao, W. C. Li, D. Qian, G. H. Wang, W. P. Zhang, T. Zhang, A. Q. Wang, F. Schüth, H. J. Bongard and A. H. Lu, *J. Am. Chem. Soc.*, 2011, **133**, 11378-11388.
10 N. Brun, S. A. Wohlgemuth, P. Osiceanu and M. M. Titirici, *Green Chem.*, 2013, **15**, 2514-2524.
11 Z. S. Wu, S. Yang, Y. Sun, K. Parvez, X. Feng and K. Müllen, *J. Am. Chem. Soc.*, 2012, **134**, 9082-9085.
12 G. C. Ruben and R. W. Pekala, *J. Non-Cryst. Solids*, 1995, **186**, 219-231.
13 D. Long, J. Zhang, J. Yang, Z. Hu, G. Cheng, X. Liu, R. Zhang, L. Zhan, W. Qiao and L. Ling, *Carbon*, 2008, **46**, 1259-1262.
14 P. Lorjai, T. Chaisuwan and S. Wongkasemjit, *J. Sol-Gel Sci. Technol.*, 2009, **52**, 56-64.
15 S. Wang, W. C. Li, L. Zhang, Z. Y. Jin and A. H. Lu, *J. Mater. Chem. A*, 2014, **2**, 4406-4412.
16 S. Mahadik-Khanolkar, S. Donthula, C. Sotiriou-Leventis and N. Leventis, *Chem. Mater.*, 2014, **26**, 1303-1317.
17 P. Katanyoota, T. Chaisuwan, A. Wongchaisuwat and S. Wongkasemjit, *Mater. Sci. Eng. B*, 2010, **167**, 36-42.
18 H. Ishida, in Handbook of Benzoxazine Resins, eds. H. Ishida and T. Agag, *Elsevier*, Amsterdam, 2011, pp. 3-81.
19 X. Ning and H. Ishida, *J. Polym. Sci., Part A Polym. Chem.*, 1994, **32**, 1121-1129.
20 P. Chutayothin and H. Ishida, *Macromolecules*, 2010, **43**, 4562-4572.
21 J. P. Randall, M. A. B. Meador and S. C. Jana, *ACS Appl. Mater. Interfaces*, 2011, **3**, 613-626.
22 H. Maleki, L. Durães and A. Portugal, *J. Non-Cryst. Solids*, 2014, **385**, 55-74.
23 X. Wang and S. C. Jana, *Polymer*, 2013, **54**, 750-759.
24 H. Guo, M. A. B. Meador, L. McCorkle, D. J. Quade, J. Guo, B. Hamilton, M. Cakmak and G. Sprowl, *ACS Appl. Mater. Interfaces*, 2011, **3**, 546-552.
25 J. Lee and G. Gould, *J. Sol-Gel Sci. Technol.*, 2007, **44**, 29-40.
26 N. Leventis, C. Sotiriou-Leventis, N. Chandrasekaran, S. Mulik, Z. J. Larimore, H. Lu, G. Churu and J. T. Mang, *Chem. Mater.*, 2010, **22**, 6692-6710.
27 J. Lee, G. Gould and W. Rhine, *J. Sol-Gel Sci. Technol.*, 2009, **49**, 209-220.
28 S. Ho Kim, M. A. Worsley, C. A. Valdez, S. J. Shin, C. Dawedeit, T. Braun, T. F. Baumann, S. A. Letts, S. O. Kucheyev, K. Jen J. Wu, J. Biener, J. H. Satcher and A. V. Hamza, *RSC Adv.*, 2012, **2**, 8672-8680.
29 S. Bandi, M. Bell and D. A. Schiraldi, *Macromolecules*, 2005, **38**, 9216-9220.
30 M. A. Meador, E. J. Malow, R. Silva, S. Wright, D. Quade, S. L. Vivod, H. Guo, J. Guo and M. Cakmak, *ACS Appl. Mater. Interfaces*, 2012, **4**, 536-544.
31 K. Yamanaka and T. Inoue, *Polymer*, 1989, **30**, 662-667.
32 J. Dunkers and H. Ishida, *Spectrochim. Acta Part A Mol. Biomol. Spec.*, 1995, **51**, 855-867.
33 H. Ishida and D. P. Sanders, *Macromolecules*, 2000, **33**, 8149-8157.
34 R. Huang, S. O. Carson, J. Silva, T. Agag, H. Ishida and J. M. Maia, *Polymer*, 2013, **54**, 1880-1886.
35 C. Tang, A. Inomata, Y. Sakai, H. Yokoyama, T. Miyoshi and K. Ito, *Macromolecules*, 2013, **46**, 6898-6907.
36 M. V. S. N. Maddipatla, D. Wehrung, C. Tang, W. Fan, M. O. Oyewumi, T. Miyoshi and A. Joy, *Macromolecules*, 2013, **46**, 5133-5140.
37 Z. Li, T. Miyoshi, M. K. Sen, T. Koga, A. Otsubo and A. Kamimura, *Macromolecules*, 2013, **46**, 6507-6519.
38 T. Miyoshi, A. Mamun and D. Reichert, *Macromolecules*, 2010, **43**, 3986-3989.
39 T. Miyoshi, O. Pascui and D. Reichert, *Macromolecules*, 2004, **37**, 6460-6471.
40 K. S. W. Sing, D. H. Everett, R. A. W. Haul, L. Moscou, R. A. Pierotti, J. Rouquerol and T. Siemieniewska, Handbook of Heterogeneous Catalysis, *Wiley-VCH Verlag GmbH & Co. KGaA*, 2008.

Table of content entry

Senlong Gu, Zhen Li, Toshikazu Miyoshi and Sadhan C. Jana*

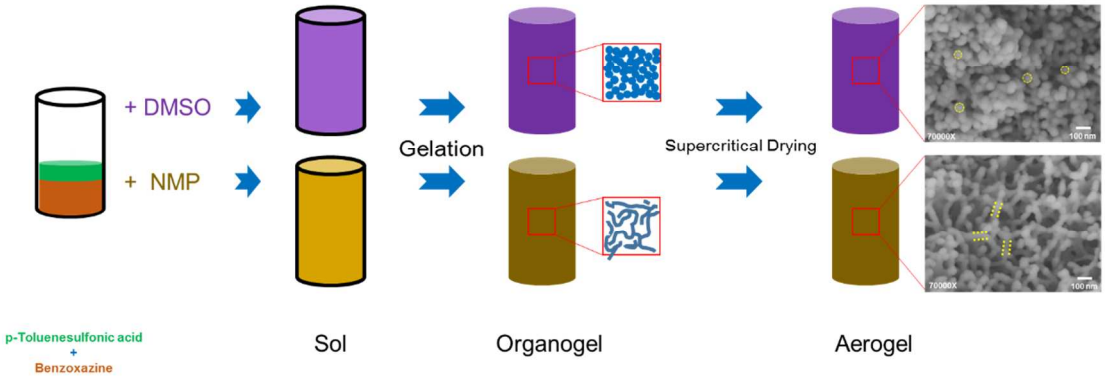

Polybenzoxazine gelation is expedited in the presence of *p*-toluenesulfonic acid and the solid networks show strong dependence on the solvent.